Chaos, Solitons and Fractals 106 (2018) 355–362

Contents lists available at ScienceDirect

Chaos, Solitons and Fractals

Nonlinear Science, and Nonequilibrium and Complex Phenomena

journal homepage: www.elsevier.com/locate/chaos

Review

Statistical properties for an open oval billiard: An investigation of the escaping basins

Matheus Hansen[a,*], Diogo Ricardo da Costa[b], Iberê L. Caldas[a], Edson D. Leonel[b]

[a] Instituto de Física da Universidade de São Paulo, Rua do Matão, Travessa R 187, Cidade Universitária, São Paulo, SP, 05314-970, Brazil
[b] Departamento de Física, UNESP - Univ Estadual Paulista, Av. 24A, 1515, Bela Vista, Rio Claro, SP, 13506-900, Brazil

ARTICLE INFO

Article history:
Received 7 June 2017
Revised 27 November 2017
Accepted 30 November 2017

Keywords:
Classical billiards
Escape of particles
Fractal boundaries

ABSTRACT

Statistical properties for recurrent and non recurrent escaping particles in an oval billiard with holes in the boundary are investigated. We determine where to place the holes and where to launch particles in order to maximize or minimize the escape measurement. Initially, we introduce a fixed hole in the billiard boundary, injecting particles through the hole and analyzing the survival probability of the particles inside of the billiard. We show there are preferential regions to observe the escape of particles. Next, with two holes in the boundary, we obtain the escape basins of the particles and show the influence of the stickiness and the small chains of islands along the phase space in the escape of particles. Finally, we discuss the relation between the escape basins boundary, the uncertainty about the boundary points, the fractal dimension of them and the so called Wada property that appears when three holes are introduced in the boundary.

1. Introduction

A billiard is a dynamical system where a point-like particle moves with constant speed along straight lines confined to a piecewise and smooth boundary where it experiences specular reflections [1]. This implies that the incidence angle must be equal to the reflection angle [1]. The study of billiards started in 1927 when Birkhoff [2] investigated the motion of particles along manifolds. After many years this scientific research has grown leading to progress in nonlinear dynamics as well as in statistical mechanics. The modern investigations of billiards are linked to the works of Sinai [3] and Bunimovich and Sinai [4,5] who made mathematical demonstrations in the topic. The billiards theory may be used to describe many different kinds of physical systems such as experiments on superconductivity [6], waveguides [7], microwave billiards [8,9], confinement of electrons in semiconductors by electric potentials [10,11], plasma physics [12] and many others.

The combination of the billiard parameters leads the phase space to exhibit three possible kinds of classification including: (i) regular/integrable; (ii) ergodic and; (iii) mixed. For the first case, the circular billiard is a typical example since its dynamics is integrable due to the conservation of energy and angular momentum [1]. The phase space is filled with straight lines (quasi periodic orbits) or a set of points (periodic orbits). Another example of such a system is the elliptical billiard in which energy and the angular momenta about the two foci are preserved [13]. Case (ii) corresponds to systems containing zero measure stable periodic orbits hence dominated by chaotic dynamics. The Bunimovich stadium [4] as well as the Sinai billiard [3] represent well this class. Finally in (iii) the phase space is composed by Kolmogorov–Arnold–Moser (KAM) islands surrounded by a chaotic sea which is limited by a set of invariant spanning curves [14,15]. The oval billiard [13] represents this class.

Berry [13] discussed a family of billiards of the oval-like shapes. The radius in polar coordinates has a control parameter ϵ which leads to a smooth transition from a circumference with $\epsilon = 0$ (integrable) to a deformed form with $\epsilon \neq 0$. For sufficiently small ϵ a special set of invariant spanning curves exists in the phase space corresponding to the so called whispering gallery orbits. They are orbits moving around the billiard close to the border with either positive (counterclockwise dynamics) or negative (clockwise dynamics) angular momentum. As soon as the parameter reaches a critical value [16], the invariant spanning curves are destroyed hence destroying the whispering gallery orbits.

Billiards can be considered for the study of recurrence of particles [17], particularly related to the Poincaré recurrence [18]. The recurrence can be measured from the injection and hence from the escape of an ensemble of particles by a hole introduced in the boundary. The dynamics is made in the following way. A particle injected through the hole is allowed to move inside the bil-

* Corresponding author.
E-mail address: mathehansen@gmail.com (M. Hansen).

https://doi.org/10.1016/j.chaos.2017.11.036
0960-0779/

liard suffering specular reflections with the boundary until it hits the hole. In this situation the particle escapes from the billiard. The number of collisions that the particle has before escaping is computed and another particle with different initial condition is introduced in the system. The dynamics is repeated until a large ensemble of particles is exhausted. For the recurrence the known results are that for a totally chaotic dynamics, the survival probability (probability that a particle survives inside of the billiard after a number of collisions with the boundary) is described by an exponential function [19,20]. However, if there are stable islands, it is possible to observe a different behavior for the survival probability. In this case, we may observe some chaotic orbits very close to stability island, and these orbits can be trapped around the islands for a long time influencing the survival probability. Therefore the survival probability is changed to a lower decay, as conjectured in Ref[18]., to be described by a power law of universal scaling with an exponent from the order of $\simeq -2.57$.

The knowledge of the structure and properties of the invariant manifolds, chaotic saddles, escape basins and their boundaries are important for the understanding and description of the anomalous transport of particles in chaotic motion for several different dynamical systems. The procedure can be applied and hence generalized to other systems including study of transport in open/closed Hamiltonian systems such as magnetically confined plasmas [21], the standard map [22] and many others. In our work, the information obtained from the investigation of escape of particles may help to give an answer, at least partially, to an open problem about the maximization or minimization of the escape of particles in billiards, see Ref.[19]. It must be emphasized that the knowledge about these structures and properties may be used in many physical applications beyond transport including applied problems in fluids [23].

In this paper we study some escaping properties for an ensemble of particles in the static oval billiard and our main goal is to understand the relation between the position of the hole in the billiard boundary and the region where the particles are injected, hence searching for a condition to maximize or minimize the escape through the hole. It is known there are preferential regions in the phase space since the density is not constant [24] and we are interested to know what are the requirements to obtain an optimization or non optimization for the escape. We then introduce a hole in the billiard boundary and studied the survival probability of particles in different positions of the hole and the region of injection of particles. It allows us to known what combinations between the position of the hole and region of the injection leads to the escape maximization. With the knowledge of the best place to get a faster escape of particles we introduce other holes in the billiard and look at the escape basin for such holes.

This paper is organized as follows. In Section 2 we discuss the model and the equations that describe the dynamics of the system. The properties of the escape are presented in Section 3. The escape of particles and the properties of the escaping basins are discussed in Section 4 while the dependence of the boundary is studied in Section 5. Our final remarks are presented in Section 6.

2. The static oval billiard

We start discussing how to obtain the equations that describe the dynamics of the system. The radius of the boundary in polar coordinate is given by

$$R(\theta, \epsilon, p) = 1 + \epsilon \cos(p\theta), \tag{1}$$

where θ is the polar coordinate, ϵ corresponds to a perturbation parameter of the circle and $p > 0$ is an integer number. For $\epsilon = 0$ the system is integrable. The phase space is foliated [1] and only periodic and quasi-periodic orbits are observed. For $\epsilon \neq 0$ the phase space is mixed containing both periodic, quasi-periodic and chaotic dynamics. When ϵ reaches the critical value [16] $\epsilon_c = 1/(1+p^2)$ the invariant spanning curves, corresponding to the whispering gallery orbits are destroyed and only chaos and periodic islands are observed. This happens when the boundary is concave for $\epsilon < \epsilon_c$ and is not observed for $\epsilon > \epsilon_c$ when the boundary exhibits segments that are convex.

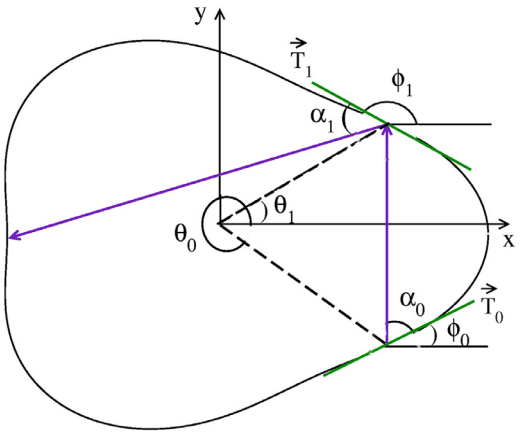

Fig. 1. Illustration of the angles involved in the billiard.

The dynamics is described by a two dimensional nonlinear mapping relating the variables $A(\theta_n, \alpha_n) \to (\theta_{n+1}, \alpha_{n+1})$ where θ denotes the polar angle to where the particle collides and α represents the angle that the trajectory of the particle makes with a tangent line at the collision point. Fig. 1 illustrates the angles and the trajectory of one particle.

For an initial condition $(\theta_n,\ \alpha_n)$ the Cartesian coordinates of the position of the particle is written as $X(\theta_n) = [1 + \epsilon\cos(p\theta_n)]\cos(\theta_n)$ and $Y(\theta_n) = [1 + \epsilon\cos(p\theta_n)]\sin(\theta_n)$. The angle of the tangent vector at the polar coordinate θ_n is $\phi_n = \arctan[\frac{Y'(\theta_n)}{X'(\theta_n)}]$, where $X'(\theta) = dX(\theta)/d\theta$ and $Y'(\theta) = dY(\theta)/d\theta$. Because there are no forces acting on the particle from collision to collision it moves along a straight line.

The trajectory is given by

$$Y(\theta_{n+1}) - Y(\theta_n) = \tan(\alpha_n + \phi_n)[X(\theta_{n+1}) - X(\theta_n)], \tag{2}$$

where θ_{n+1} is obtained numerically and corresponds to the new polar coordinate of the particle when it hits the boundary. The angle α_{n+1} gives the slope of the trajectory of the particle after a collision and is calculated as

$$\alpha_{n+1} = \phi_{n+1} - (\alpha_n + \phi_n). \tag{3}$$

The final form of the mapping is then given as

$$A: \begin{cases} F(\theta_{n+1}) & = Y(\theta_{n+1}) - Y(\theta_n) - \tan(\alpha_n + \phi_n) \\ & \times [X(\theta_{n+1}) - X(\theta_n)], \\ \alpha_{n+1} & = \phi_{n+1} - (\alpha_n + \phi_n), \end{cases} \tag{4}$$

where θ_{n+1} is obtained numerically from $F(\theta_{n+1}) = 0$ and the angle of the tangent vector at the polar coordinate θ_{n+1} is $\phi_{n+1} = \arctan[\frac{Y'(\theta_{n+1})}{X'(\theta_{n+1})}]$.

In Fig. 2(a) we show an example of the boundary and collisions for a chaotic orbit from the chaotic sea of the phase space, shown in Fig. 2(b), while Fig. 2(c) corresponds to a periodic orbit of a particle inside of the stability island of Fig. 2(b). The control parameters used were $p = 3$ and $\epsilon = 0.08 < \epsilon_c$.

3. The relation between injection and escaping region

In this section we discuss some statistical properties for the escape of particles considering two holes placed on the boundary, with constant angular aperture size of $h = 0.20$ measured in the

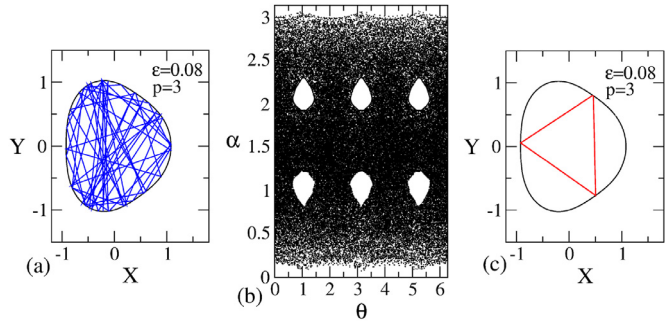

Fig. 2. (a) Trajectory of the particle collisions in the billiard for the chaotic orbit shown in (b) while (c) shows a period three orbit inside the stability island in the lower chain seen in (b).

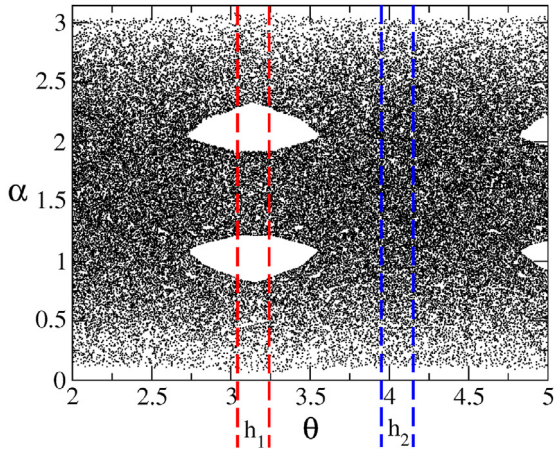

Fig. 3. Illustration of the positions of the holes h_1 and h_2, with $\epsilon = 0.08$ and $p = 3$.

polar angle θ. The position for the holes are $h_1 \in (3.04, 3.24)$ corresponding to a region with chaotic and regular areas (mixed structure) and $h_2 \in (3.95, 4.15)$ located at a completely chaotic region as shown in Fig. 3. There is an interesting difference about the escape rate for the holes h_1 and h_2. There are preferential regions to place a hole along the boundary to observe escape of particles faster than the others. The escape rate of particles when the hole is placed in chaotic regions is larger than those placed in regions where stability islands are present [24]. Therefore h_2 leads to a faster escape as compared to h_1.

To give convincing arguments on that, we first keep h_1 open while h_2 is closed. An ensemble of 10^4 particles from h_1 is injected and the dynamics of each particle is running to, at most, 10^6 collisions with the boundary using mapping (4). The initial conditions are uniformly distributed in a window of 10^2 θ_0 values in the interval (3.04, 3.24) or (3.95, 4.15) and 10^2 α_0 values in the interval $(0, \pi)$. Our statistics are made in terms of the number of collisions n of each particle until it escapes. Every time an initial condition hits $h_1(h_2)$, the particle escapes, we interrupt the simulation and other initial condition is initialized. The process is repeated until the whole ensemble is exhausted. We compute the survival probability $P(n)$, that corresponds to the number of particles that do not escape through the hole until collision n. The survival probability is given by

$$P(n) = \frac{1}{N} N_{surv}(n), \tag{5}$$

where N is the number of initial conditions and N_{surv} is the number of the particles that survived until the nth collision. Fig. 4(a) shows the results of the survival probability obtained for $\epsilon = 0.08$, $\epsilon = 0.1$, $\epsilon = 0.12$ and $p = 3$ and for an ensemble of 10^4 different particles. The decay of the survival probability is exponential and can be described by

$$P(n) = P_0 e^{n\delta}, \tag{6}$$

where P_0 is a constant, δ is the slope of the decay and n is the number of collisions with the boundary. For such configuration an exponential fitting obtained $P(n)$, as shown in Fig. 4(a), gives $\delta_{h_1 \to h_1} = -0.0188(7)$. When the process above is repeated, but now, with h_1 closed and h_2 open, the average decay of $P(n)$ is faster as compared to the earlier case, as shown in Fig. 4(b). An exponential fit for this case gives $\delta_{h_2 \to h_2} = -0.0437(3)$ confirming the faster escape from h_2 while compared to h_1. Although the size of the holes h_1 and h_2 are the same in polar angle, their corresponding arc length S_1 and S_2 has ratio $S_1/S_2 \cong 0.87$, which does not produce qualitative modifications in the approach used in the present configuration of the model.

We notice the importance of the position of the hole for the maximization or minimization of the escape of particles. Our results confirm that injecting particles through a hole placed in a chaotic region leads to a faster escape rate while compared to the particles injected through a hole placed in a region with mixed structures. The two questions we want to address: Are there preferential regions to inject the particles to maximize or minimize the escape? Are there a relation among the injection regions and the positions to place the holes for a faster or lower escape rates?

To answer these questions, we inject particles from h_2 (a chaotic region) and allow the particles to escape only from h_1 (region that represents a mix structure). The procedure to inject the particles, the number of initial conditions and the number of collisions that each particle is allowed to live are the same as described before. Fig. 4(c) shows the survival probability $P(n)$ for such configuration. The average fitting gives $\delta_{h_2 \to h_1} = -0.0183(4)$ which is quite close to $\delta_{h_1 \to h_1} = -0.0188(7)$ as obtained earlier. If the particles are injected from h_1 and the escape is measured from h_2 a significant change in the survival probability is observed as shown in Fig. 4(d). The survival probability $P(n)$ does not decay to zero anymore. It rather decays for n about $n \simeq 10^2$ and then converges to a constant plateau, which can be explained by two reasons: (1) initial conditions inside of the periodic islands that are forbidden to escape and; (2) very long stickiness observed for orbits visiting regions very close to the stability islands. It is interesting to notice the number of particles that remain in the plateau decreases when the parameter ϵ is increased. The size of the islands in such region decreases indicating that less initial conditions have been taken into the regions near the islands. As soon as the parameter ϵ is changed the structure of the phase space changes, therefore, the size of the islands change, islands and the whispering gallery orbits may be destroyed. Even considering all of these possible changes the behavior of the survival probability apparently does not suffer changes when we study the escape of particles in regions totally chaotic or with mixed structure.

An immediate conclusion is that a faster escape is produced by conditions where particles are injected in the chaotic sea while the hole is also placed in the chaotic sea. Therefore the position of the hole for the escape of particles has important influence to the maximization or minimization of the escape of particles. However, the determining factor is the region of injection of particles. As we show, the best results for the escape of particles comes with the choice of the chaotic regions to inject the particles.

We stress that no connection between the hole h_1 and h_2 existed. Interested reader can see results of connected holes in [25].

4. Escape basins investigation

In this section we discuss the escape of particles in the static oval billiard in the presence of two holes in the boundary starting the dynamics in the best scenario of escape, i.e., in the chaotic sea.

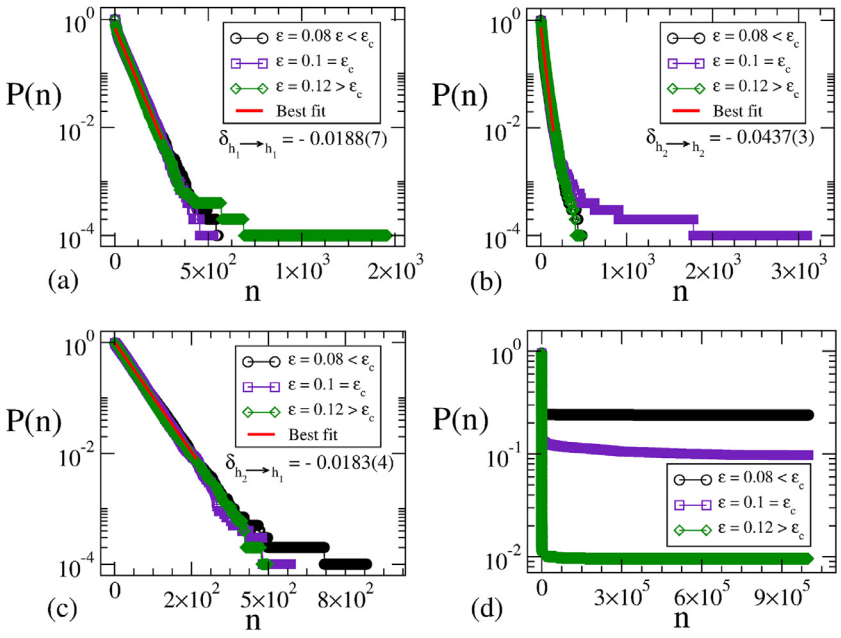

Fig. 4. Plot of the survival probability for: (a) the particles are injected through the hole h_1; (b) the particles are injected through the hole h_2; (c) when the particles are injected from the region of h_2 and escape through h_1 and (d) when the particles are injected from the region of h_1 and escape through h_2. The parameters used are $p = 3$ and $\epsilon = 0.08$, $\epsilon = 0.1$ and $\epsilon = 0.12$.

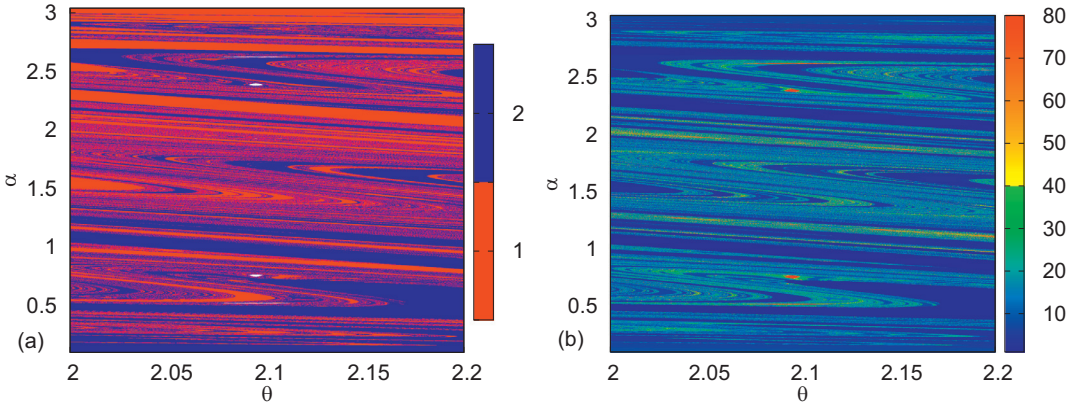

Fig. 5. (a) The escape basins for the particles that escape through the hole h_1 (red color), h_2 (blue color) and for the particles that do not escape (white color); (b) the same escape basin of (a), but with the color scale with the number of collisions until escape. The used parameters are $\epsilon = 0.08$ and $p = 3$. (For interpretation of the references to colour in this figure legend, the reader is referred to the web version of this article.)

We inject an ensemble of 4×10^6 particles from the chaotic sea evolving the dynamics of each particle up to 10^6 collisions with the boundary. The initial conditions were uniformly distributed in a window of 2×10^3 for $\theta_0 \in (2.0, 2.2)$ and 2×10^3 for $\alpha_0 \in (0, \pi)$. We keep two holes in the boundary placed at $h_1 \in (0.1, 0.3)$ and $h_2 \in (3.95, 4.15)$. The idea is to construct the basin of escape for each initial condition. Given an initial condition, as soon as its orbit escapes the following information is obtained: to what hole the escape happened, if h_1 or h_2 and the number of collisions at the escape. After a particle escapes a new initial condition is started and so on until all the ensemble is exhausted. If an orbit does not escape, this information is also retained.

Fig. 5(a) shows a plot of the configuration α *vs.* θ where each point denotes the initial condition. The color identifies to what hole the injected orbit escape through. A escape through h_1 is painted red while blue identifies escape through h_2. White color implies no escape up to 10^6 collisions. This plot corresponds to a basin of escape. We notice from Fig. 5(a) that, there are some regions where the particles do not escape through any hole, for example, near the region $(\theta, \alpha) = (2.1, 0.75)$. Immediate questions are: what is the reason for such behavior? What kind of phenomenon could be acting in this region? To answer these questions we analyze the basin of escape using a color scaling to have an insight of the number of collisions with the boundary each particle spent until escaping, as shown in Fig. 5(b). We constructed again the basin of escape but now using as maximum length of number of collisions 80. We see that the majority of particles escape very fast, namely before 40 collisions with the boundary. Some of them live longer and a small amount survive until 80 collisions. A magnification of the red region of Fig. 5(b) is shown in Fig. 6(a). As soon as the initial conditions get apart from the red region, the escape gets faster. The initial conditions in the red regions suffer two types of dynamics. Some of them are indeed inside a periodic island, therefore are forbidden to escape such region. If the hole is placed outside of the island, the escape never takes place. The other set of initial conditions are outside of the island, but very close to it. They suffer strong influence of the stickiness staying trapped near it for long time, as shown in Fig. 6(b). The particles

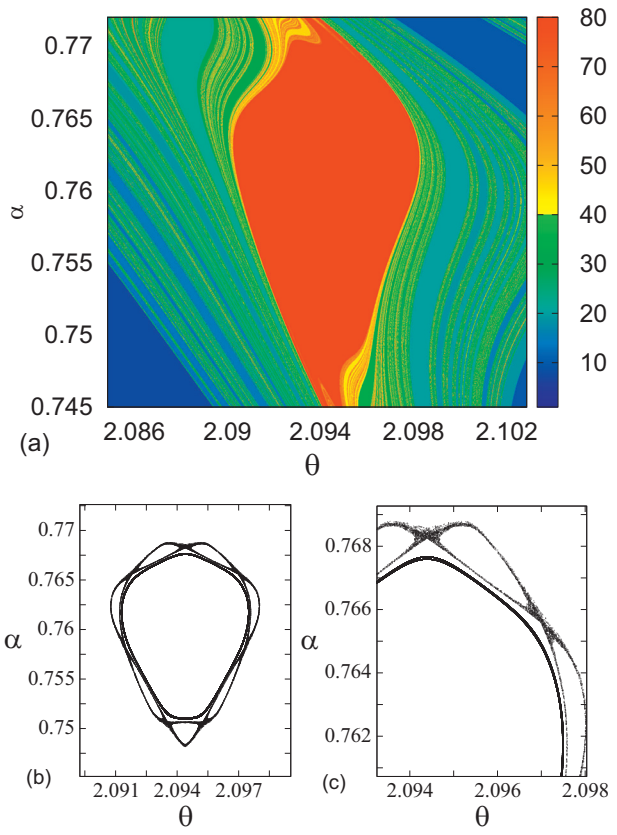

Fig. 6. (a) Magnification of the chain of islands in the plane α *vs.* θ; (b) The representation of the chain of islands in the phase space; (c) Observation of the stickiness phenomenon around the islands. The parameters used are $\epsilon = 0.08$ and $p = 3$. (For interpretation of the references to colour in this figure legend, the reader is referred to the web version of this article.)

undergo a large number of collisions until they get rid of the stickiness. Fig. 6(c) shows a magnification of Fig. 6(b).

We see from Fig. 6(a) there are chains along the plane α *vs.* θ to where the particles move and that they resemble to manifolds. Then we investigate the behavior of stable and unstable manifolds from a saddle fixed point. An unstable (stable) manifold is a set of points that moves away (approaches) to the saddle fixed point under the forward (backward) iterations of the map, as time goes to infinity. To construct the manifolds we used a numerical technique called as *sprinkler method* [26,27]. The method consists in splitting the phase space along the region of interest into a fine grid of points and iterate each point n times. After a certain number of collisions each point leaves the grid and starts to follow the manifold hence giving a good approximation of the stable and unstable manifolds. Fig. 7(a) and (b) shows plots of the unstable and stable heteroclinic manifolds for the saddle fixed point ($\theta^* \approx 2.0522$, $\alpha^* \approx 0.9997$) (purple point) indicated in the figure.

A chaotic saddle is defined as a set of points (that has zero Lebesgue measure [28]) form by the intersection of the stable and unstable manifolds from the saddle fixed points. The points that belong to the chaotic saddle remain there for all iterations of the map. When initial conditions start closer to the chaotic saddle, they wander along the unstable manifold in an almost erratic way approaching arbitrarily close to the unstable manifold in the chaotic saddle. Therefore if an initial condition injected in the dynamics lives near a chaotic saddle it shall undergoes a large number of collisions until finding a route to escape through the holes.

To elucidate the influence of the chaotic saddle in the escape of particles we made a magnification of Fig. 5(b) considering the larger time of dynamics as 200 collisions as shown in Fig. 8(a). We notice many points undergo around 50 collisions with the boundary and when we compare these regions with the chaotic saddle, as shown in Fig. 8(b), the position of many points that undergo more collisions with the boundary are very close to the chaotic saddle. This is indeed the reason why some points undergo more collisions with the boundary than others to escape, hence reinforcing the influence of stickiness close to the chains and the chaotic saddle.

5. Escape basins properties

In the previous section we saw the intricate relation of the escaping basin containing many intertwined chains as shown in Fig. 5(a) for the escape basins of the holes h_1 and h_2. To investigate the uncertainty of the initial condition to what hole it escapes in Fig. 5(a), we used the so called uncertain fraction method [29,30]. The method consists of taking an initial condition (θ_0, α_0) and following it in time checking to what hole it escaped. Then a small perturbation ζ is added to the initial condition along the range $(\theta_0 + \zeta, \alpha_0)$ and $(\theta_0 - \zeta, \alpha_0)$. From there we follow the evolution of such initial condition and seek if the escaping hole is the same or not as the initial condition without perturbation.

The process is repeated for a large number of initial conditions N_T where the index T identifies total initial conditions. Defining N_u as the number of uncertain initial conditions we obtain a fraction of uncertain initial conditions as $f(\zeta) \approx N_u/N_T$. For different values of ζ, we notice the uncertain fraction scales with ζ as a power law $f(\zeta) \sim \zeta^{\mu}$ where μ is the uncertainty exponent of the escape basin boundary. If the boundary is smooth, $f(\zeta) \sim \zeta$ since the uncertain conditions occupy a strip of width 2ζ in the boundary. However for fractal boundaries, the uncertainty exponent scales with $f(\zeta) \sim \zeta^{\mu}$, where $0 < \mu < 1$ is the uncertainty exponent.

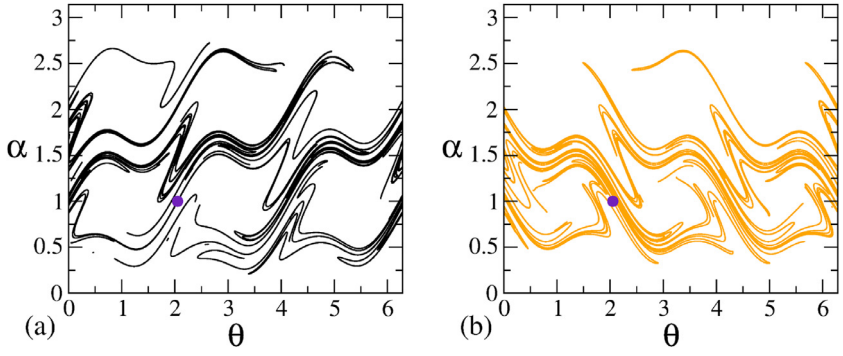

Fig. 7. (a) Plot of the unstable manifold of the saddle point ($\theta^* \approx 2.0522$, $\alpha^* \approx 0.9997$); (b) Plot of the stable manifold for the same saddle fixed point of (a). The parameters used are $\epsilon = 0.08$ and $p = 3$.

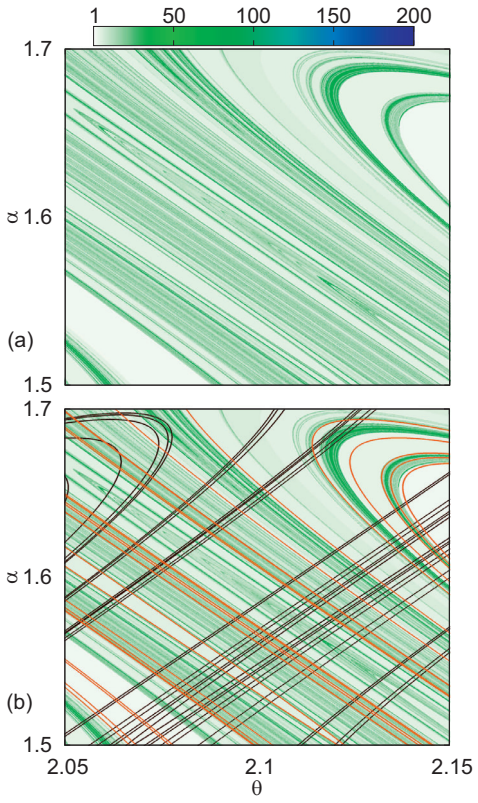

Fig. 8. (a) Amplification of Fig. 5(b) with a largest escape time of 200 collisions. (b) Chaotic saddle influence: particles near stable (orange) and unstable (black) manifold crossings have a higher scape time. The parameters used are $\epsilon = 0.08$ and $p = 3$. (For interpretation of the references to colour in this figure legend, the reader is referred to the web version of this article.)

The results for the uncertainty exponent, are shown in Fig. 9(a) and (b) as a function of different values of ζ. For the forward iterations (when $(\theta_0 + \zeta, \alpha_0)$) we obtained $\mu = 0.1203(5)$ while for the backward iterations (for $(\theta_0 - \zeta, \alpha_0)$) we found $\mu = 0.1201(5)$. The uncertainty exponent μ can be related to the box-counting boundary dimension D_0 via the relation $\mu = D - D_0$, where D is the dimension of the phase space, in our case $D = 2$. Using the uncertain exponent for forward iterations we obtained that the escape basin boundary dimension is $D_0 = 1.8797(5)$ while for backward iterations is $D_0 = 1.8799(5)$. Therefore the escape basin boundary has a fractal dimension from the order of $D_0 = 1.8798(5)$.

To better understand the behavior of the boundaries of the escape basins we analyze how the uncertainty exponent behaves when the size of the holes h_1 and h_2 are increasing/decreasing. In Fig. 9(c) we see that μ obeys a power law of the hole size. Smaller holes lead to smaller values of μ. The opposite is also observed, as larger the hole size is, larger the value of μ will be. This behavior shows that when the holes are small the boundaries of the escape basins become very complicate which will give a fractal dimension $D_0 \approx 2$. In other words, when the size of the holes became large, the fractal dimension D_0 approaches the unity, leading the boundaries of the escape basins to a less complicated form, say *smother*, where the boundaries begin to approach their simplest form.

After considering a transformation in Fig. 9(c) ($h \longrightarrow h/\epsilon$) all curves are overlapped onto each other onto a single curve, that is described by a power law $\mu \sim h^{\rho}$, as shown in Fig. 9(d). The slope obtained, by a power law fit, was $\rho = 0.9658(1)$.

When a third hole is introduced in the boundary the so called Wada property [29,31] can be explored. The property shows there are points in the basin boundary that belong to the three escape basins. To introduce a mathematical definition of Wada property (see Refs. [32,33]) we initially consider that a point P is a boundary point of an escape basin β if every open neighborhood of P intersects the basin β and at least another basin. The basin boundary is the set of all boundary point of that basin. The boundary point P is a Wada point if every open neighborhood of P intersects at least three different basins. A basin boundary exhibits Wada property if

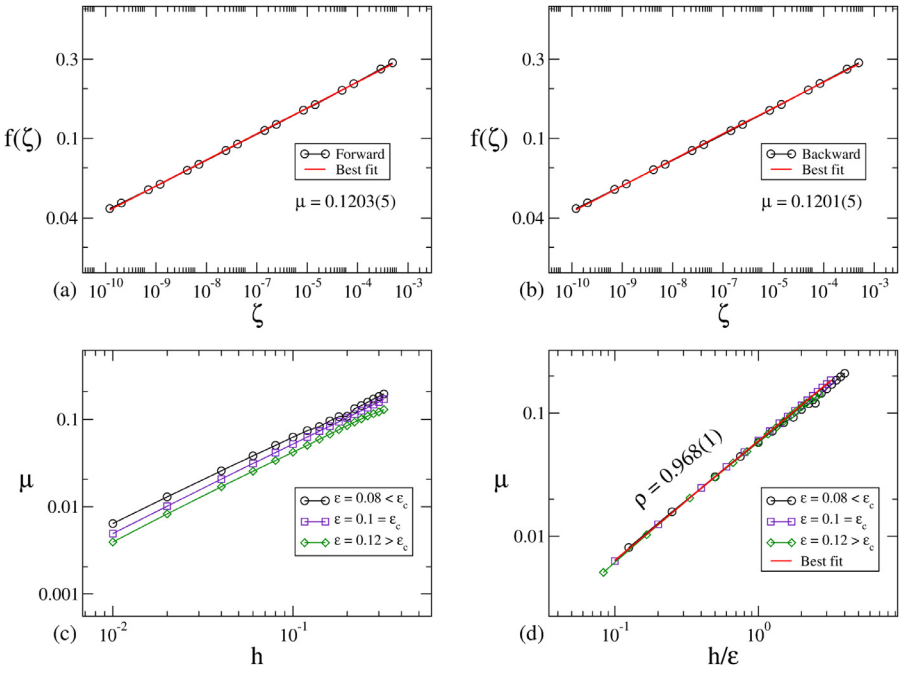

Fig. 9. (a) Plot of $f(\zeta)$ *vs.* ζ. A power law fitting gives the uncertain exponent $\mu = 0.1203(5)$ for forward iterations; (b) Plot of $f(\zeta)$ *vs.* ζ with the uncertainty exponent $\mu = 0.1201(5)$ for backward iterations; (c) the relation between the uncertainty exponent and the size h of the hole and (d) the overlap onto a single and hence universal plot after a transformation $h \longrightarrow h/\epsilon$. The parameters used are $p = 3$ and $\epsilon = 0.08$, $\epsilon = 0.1$ and $\epsilon = 0.12$.

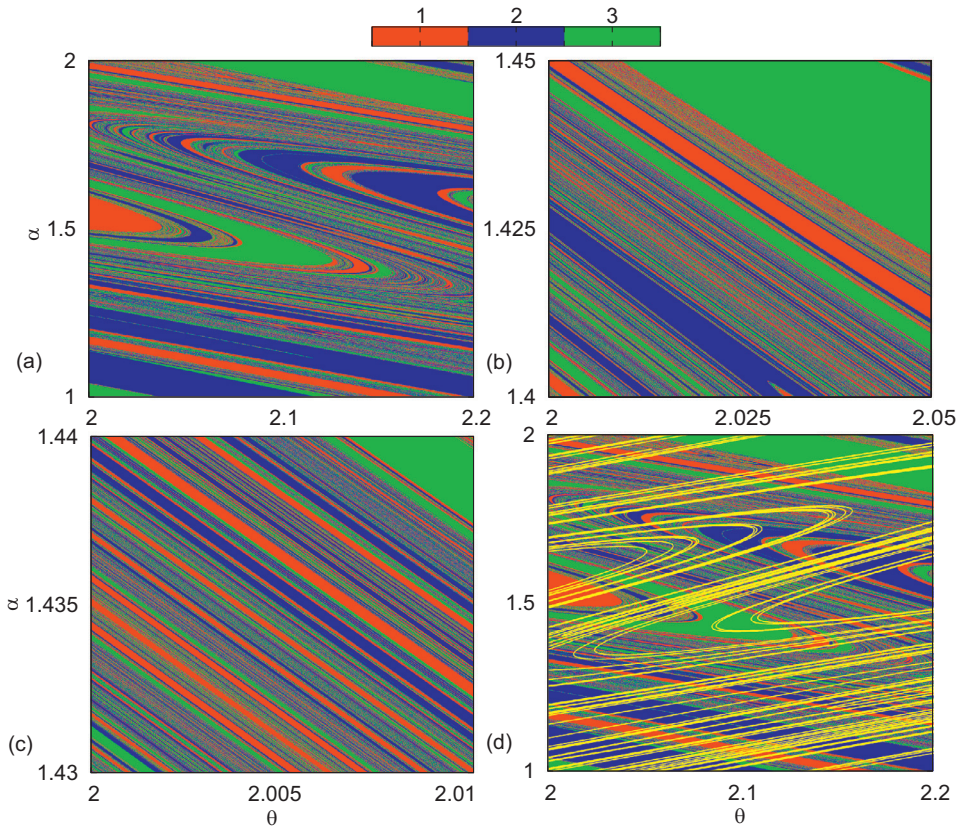

Fig. 10. (a) Plot of the escape basins for the particles escaping from h_1 (red color), h_2 (blue color) and h_3 (green color); (b) Magnification of the (a); (c) Magnification of (b); (d) Plot of the unstable (yellow line) manifold together with the basins of escape. The parameters used are $\epsilon = 0.08$ and $p = 3$. (For interpretation of the references to colour in this figure legend, the reader is referred to the web version of this article.)

every boundary point of β is a Wada point, such that boundary of such a basin is a Wada basin boundary [26,27].

To observe the Wada property we need first to introduce one more hole in the boundary. We place it at $h_3 \in (6.0, 6.2)$ along the chaotic sea. Fig. 10(a) shows how the escaping basins are distributed in the phase space. Escape from h_3 is represented in green color.

The Wada property warrants the stripes of all basins coexist in an increasingly finer scale as shown in Fig. 10(b) and (c). This Illustration of the Wada property does not guarantee the existence of the property. To have a confirmation of the Wada property an unstable manifold of an unstable periodic point P must intersects every basin of escape. This can be seen in Fig. 10(d) where the unstable manifold intersects the three escape basins. If an unstable manifold of a periodic orbit P belongs to any escape basin and intersects all the escape basins then the Wada property is satisfied.

6. Discussion and conclusions

As a short summary, we study the behavior of the escape of particles in an oval static billiard with holes on the boundary. We investigated the behavior of the survival probability of the particles. This gives us information about the number of particles that remain inside of the billiard after a number of collisions among the particles and the boundary in different scenarios of injection. We noticed, when both the injected particles and hole are placed in the chaotic sea, a maximization of escape is observed when compared to any other configuration of injection or hole position. This information helps to understand how to get or not an escape maximization. Even in the best scenario of escape of particles the existence of stickiness and chaotic saddle may influence some particles and make their escape lower than others. With two holes in the boundary we proved that the basins boundary are very complex and through the uncertainty in the initial conditions, we found a fractal dimension for the escape basins boundaries. The presence of three holes in the boundary leads to the Wada property to be observed in initial configuration space.

Acknowledgments

MH thanks to CAPES for the financial support. DRC acknowledges support from Brazilian agencies PNPD/CAPES and FAPESP under the grant 2013/22764-2. ILC acknowledges support from Brazilian agency FAPESP under the grant 2011/19296-1. EDL acknowledges support from the Brazilian agencies FAPESP under the grants 2017/14414-2, 2014/00334-9 and 2012/23688-5 and CNPq through the grants 306034/2015-8 and 303707/2015-1.

References

[1] Chernov N, Markarian R. Chaotic billiards. American Mathematical Society; 2006.
[2] Birkhoff G. Dynamical systems. Providence, RI, USA: American Mathematical Society; 1927.
[3] Sinai YG. Dynamical systems with elastic reflections. Russ Math Surv 1970;25:137.
[4] Bunimovich LA. On ergodic properties of certain billiards. Funct Anal Appl 1974;8:73.
[5] Bunimovich LA, Sinai YG. Statistical properties of lorentz gas with periodic configuration of scatterers. Commun Math Phys 1981;78:479.
[6] Graf HD, et al. Distribution of eigenmodes in a superconducting stadium billiard with chaotic dynamics. Phys Rev Lett 1992;69:1296.
[7] Persson E, et al. Observation of resonance trapping in an open microwave cavity. Phys Rev Lett 2000;85:2478.
[8] Stein J, Stokmann HJ. Experimental determination of billiard wave functions. Phys Rev Lett 1992;68:2867.

[9] Stokmann HJ. Quanum chaos: an introduction. Cambridge University Press; 1999.
[10] Sakamoto T, et al. Electron focusing in a widely tapered cross junction. Jpn J Appl Phys 1992;30. L1186.
[11] Bird JP. Recent experimental studies of electron transport in open quantum dots. J Phys Condens Matter 1992;11:R413.
[12] Neishtadt AI, Artemyev AV. Destruction of adiabatic invariance for billiards in a strong nonuniform magnetic field. Phys Rev Lett 2012;108:064102.
[13] Berry MV. Regularity and chaos in classical mechanics, illustrated by three deformations of a circular 'billiard'. Eur J Phys 1981;2:91.
[14] Lichtenberg AJ, Lieberman MA. Regular and chaotic dynamics, applied mathematical sciences, 38. New York: Springer-Verlag; 1992.
[15] Reichl EL. The transition to chaos, conservative classical systems and quantum manifestations. Springer; 2004.
[16] Oliveira DFM, Leonel ED. On the dynamical properties of an elliptical-oval billiard with static boundary. Commun Nonlinear Sci Numer Simulat 2010;15:1092.
[17] Demers M, Wright P, Young L-S. Escape rates and physically relevant measures for billiards with small holes. Commun Math Phys 2010;294:353.
[18] Altmann EG, Tél T. Poincar recurrences and transient chaos in systems with leaks. Phys Rev E 2009;79:016204.
[19] Dettmann CP. Recent advances in open billiards with some open problems. Frontiers in the study of chaotic dynamical systems with open problems. Elhadj Z, Sprott JC, editors. World Scientific; 2011.
[20] Demers M. Dispersing billiards with small holes, in ergodic theory, open dynamics and coherent structures. Springer proceedings in mathematics; 2014.
[21] Mathias AC, Viana RL, Kroetz T, Caldas IL. Poincaré recurrences and transient chaos in systems with leaks. Physica A 2017;469:681.
[22] Sanjuán MF, Horita T, Aihara K. Opening a closed hamiltonian map. Chaos 2003;13:17.
[23] Neufeld Z, Haynes PH, Picard G. The effect of forcing on the spatial structure and spectra of chaotically advected passive scalars. Phys Fluids 2000;12:2506.
[24] Hansen M, de Carvalho RE, Leonel ED. Influence of stability islands in the recurrence of particles in a staticoval billiard with holes. Phys Lett A 2016;380:3634.
[25] Naplekov DM, Yanovsky VV. Billiard with a handle. Phys Rev E 2016;94:042225.
[26] Poon L, Campos J, Ott E, Grebogi C. Wada basin boundaries in chaotic scattering. Int J Bifurcation Chaos 1996;6:251.
[27] da Silva EC, Caldas IL, Viana RL, Sanjuán MAF. Escape patterns, magnetic footprints, and homoclinic tangles due to ergodic magnetic limiters. Phys Plasmas 2002;9:4917.
[28] Grebogi C, Ott E, Yorke JA. Crises, sudden changes in chaotic attractors and transient chaos. Physica D 1983;7:181.
[29] Alligood KT, Sauer TD, Yorke JA. CHAOS an introduction to dynamical systems. New York: Springer-Verlag; 2012.
[30] Mcdonald SW, Grebogi C, Ott E, Yorke JA. Fractal basin boundaries. Physica D 1985;17:125.
[31] Aguirre J, Viana RL, Sanjuán MAF. Fractal structures in nonlinear dynamics. Rev Mod Phys 2009;81:333.
[32] Nusse HE, Yorke JA. Basin of attraction. Science 1996;271:1376.
[33] Nusse HE, Yorke JA. Wada basin boundaries and basin cells. Physica D 1996;90:242.